

Dalton Transactions

Accepted Manuscript



This is an *Accepted Manuscript*, which has been through the Royal Society of Chemistry peer review process and has been accepted for publication.

Accepted Manuscripts are published online shortly after acceptance, before technical editing, formatting and proof reading. Using this free service, authors can make their results available to the community, in citable form, before we publish the edited article. We will replace this *Accepted Manuscript* with the edited and formatted *Advance Article* as soon as it is available.

You can find more information about *Accepted Manuscripts* in the [Information for Authors](#).

Please note that technical editing may introduce minor changes to the text and/or graphics, which may alter content. The journal's standard [Terms & Conditions](#) and the [Ethical guidelines](#) still apply. In no event shall the Royal Society of Chemistry be held responsible for any errors or omissions in this *Accepted Manuscript* or any consequences arising from the use of any information it contains.

Antenna Effect in Truxene-bridged BODIPY Triarylzinc(II)porphyrin Dyads: Evidence for a Dual Dexter-Förster Mechanism

Hai-Jun Xu,^a Antoine Bonnot,^b Paul-Ludovic Karsenti,^b Adam Langlois,^b Mohammed Abdelhaleem,^b Jean-Michel Barbe,^a Claude P. Gros,^{*a} and Pierre D. Harvey^{*a,b}

^a Institut de Chimie Moléculaire de l'Université de Bourgogne (ICMUB, UMR 6302), Université de Bourgogne, Dijon, France. Fax: 33 (0)3 80 39 61 17; Tel: 33 (0)3 80 39 61 12; E-mail: claude.gros@u-bourgogne.fr

^b Département de Chimie, Université de Sherbrooke, Sherbrooke, PQ, Canada, J1K 2R1. Fax: 819 821 8017; Tel: 819 821 7092; E-mail: pierre.harvey@USherbrooke.ca

Received (in XXX, XXX) Xth XXXXXXXXXX 20XX, Accepted Xth XXXXXXXXXX 20XX
DOI: 10.1039/b000000x

Abstract. The antenna process from an energy donor (BODIPY; 4',4'-difluoro-1',3',5',7'-tetramethyl-4'-bora-3a',4a'-diazas-indacene) in its singlet state to two acceptors (two zinc(II) 5,15-*p*-tolyl-10-phenylporphyrin) bridged by a central truxene residue (5',5'',10',10'',15',15''-hexabutyltruxene), **5**, has been analysed by means of comparison of the energy transfer rates with those of a structurally similar β -substituted BODIPY-(zinc(II) 5,10,15-*p*-tolylporphyrin), **6**, where no conjugation is present between the donor and the two acceptors using the Förster Resonance Energy Transfer approximation (FRET). It is estimated that the energy transfer in **5** operates mostly *via* a Dexter mechanism (>99%), and the remainder proceeds *via* a Förster mechanism (<1%). This information is useful for the design of future molecular devices aimed at harvesting light.

Introduction

Boron-dipyrins (BODIPY)/metalloporphyrin dyads and assemblies are a relatively novel class of compounds that can exhibit rich antenna effects namely the singlet energy transfers, as well as electron transfer when in the presence of an electron acceptor such as fullerene derivatives.¹⁻³ Their conjugates have recently been the subject of a comprehensive review.⁴ The investigation of the energy transfer processes from BODIPY donors to porphyrin and metalloporphyrin acceptors or from porphyrin and metalloporphyrin donors to azaBODIPY, and blue-BODIPY (boron-dipyrinbisteryl) acceptors are still attracting a lot of attention.⁵⁻¹² In this respect, we also recently studied BODIPY/metalloporphyrin conjugates including compound **6** (Chart 1).¹³ The absence of conjugation in the -O-CH₂-bridges holding BODIPY donor and the tetraarylzinc(II)-porphyrin acceptors makes the dyad prone to operate *via* a through space Förster mechanism.¹⁴ However, dyads built upon a BODIPY-bridge-metalloporphyrin where the bridge is a conjugated spacer, such as -C₆H₄-C≡C-C₆H₄- for example, brings in the possibility of a second mechanism, a through bond Dexter mechanism (double electron exchange),¹⁵ which relies on orbital overlaps that occurs in conjugated bridges.

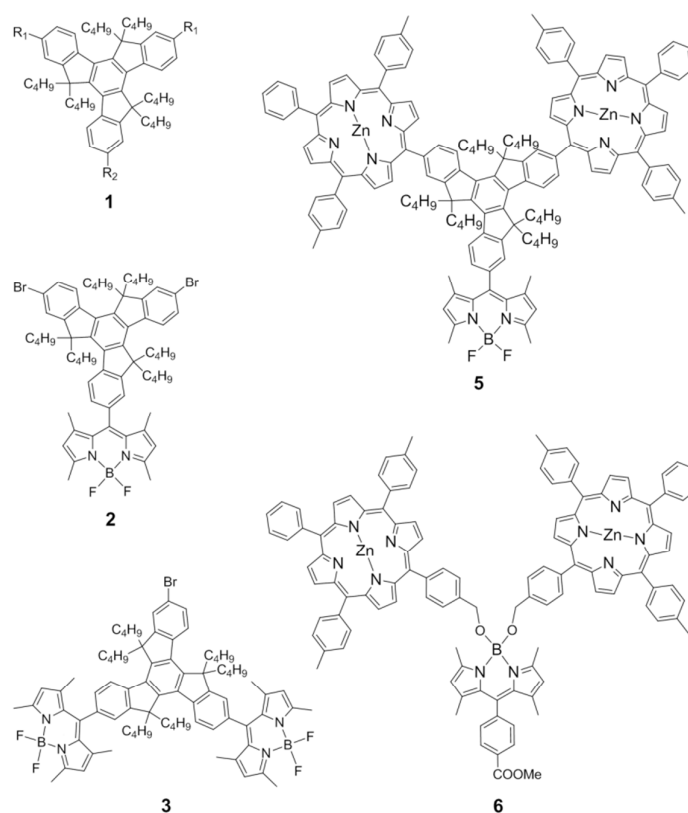


Chart 1. Structures of the investigated chromophores and dyads.

Truxenes (see general structure **1** in Chart 1),^{16, 17} are examples of aromatics around which various residues can be linked. Recently, our groups and others reported a series of truxene-containing dyads,^{18,19} oligomers^{20,21} and polymers,²²⁻²⁴ in which both singlet and triplet energy transfers take place. Because of this intrinsic property, this aromatic frame appears as a conjugated platform promoting energy transfers between chromophores anchored at the periphery of the triangular aromatic as evidenced by the literature.²⁵⁻³⁰ Truxene is prone to promote singlet energy transfer *via* a Dexter mechanism but does not preclude the Förster one. The duality of the two processes has been pointed out and sometimes analysed before for different dyads.^{31,32} However, such a study requires an in-depth investigation and consequently such topic is not particularly common. The knowledge of the mechanism and its relative efficiency are key information in the design of materials dedicated to photonics such as solar cells and light emitting diodes.

We now report the synthesis of a truxene-based dyad, for which the donor and acceptors are respectively BODIPY and two tetraarylzinc(II)porphyrins, compound **5**, which bears a structural resemblance with compound **6**, here supported by modeling. The difference in rate for singlet energy transfers, k_{ET} , between dyad **5** (Dexter and Förster) and dyad **6** (Förster), and adapting for the different structural parameters, allow estimating the contribution of the Dexter process *vs* the Förster one in compound **5**. This contribution is > 99% (Dexter), which is consistent with the direct linkage between the donor and acceptors but at the same time, indicates its clear dominance.

Experimental section

Materials. Unless otherwise noted, all chemicals and solvents were of analytical reagent grade and used as received. Absolute dichloromethane (CH_2Cl_2) was obtained from Carlo Erba. Silica gel (Merck; 70-120 mm) was used for column chromatography. Analytical thin-layer chromatography was performed with Merck 60 F₂₅₄ silica gel (precoated sheets, 0.2 mm thick). Reactions were monitored by thin-layer chromatography, UV/Vis spectroscopy and MALDI/TOF mass spectrometry. Di- (**1a**) or monocarbaldehydhexabutyltruxene (**1b**) were prepared as previously described in the literature.^{18,19} Borolanylporphyrin **4** was prepared following a recently reported procedure.³³

4,4-Difluoro-8-(5',5'',10',10'',15',15''-hexabutyl-7',12'-dibromotruxene)-1,3,5,7-tetramethyl-4-bora-3a, 4a-diaza-s-indacene (2). 2,4-Dimethylpyrrole (4 mmol, 0.38 g, 412.0 μL) and 5,5',10,10',15,15'-hexabutyl-7,12-dibromotruxene-2-dicarbaldehyde (2 mmol, 1.728 g) were dissolved in 100 mL of dry CH_2Cl_2 under N_2 atmosphere. 50 μL of TFA was

added at room temperature and the solution was stirred overnight until TLC-control showed the complete consumption of the starting aldehyde. At this point, DDQ (2 mmol, 0.454 g) was added, stirring was continued for 60 min followed by the addition of 6 mL of Et₃N and 6 mL of BF₃·OEt₂ respectively. After stirring for 30 min the reaction mixture was washed with water, dried over Na₂SO₄ and evaporated to dryness. The residue was purified by column chromatography on silica gel with 60% DCM-heptane to afford the title compound in 17% yield (369.0 mg). ¹H NMR (CDCl₃) δ (ppm): 8.50 (d, 1 H, truxene-*H*), 8.22 (d, 2 H, truxene-*H*), 7.61 (m, 2 H, truxene-*H*), 7.55 (m, 2 H, truxene-*H*), 7.46 (m, 1 H, truxene-*H*), 7.33 (m, 1 H, H-pyrro), 6.04(s, 2 H, H-pyrro), 3.00 (m, 6 H, H-truxene), 2.61 (s, 6 H, pyrro-CH₃), 2.10 (m, 6 H, Truxene-CH₂-), 1.49 (s, 6 H, pyrro-CH₃) 0.936 (m, 12 H, -CH₂-), 0.75-0.45(m, 30 H, -CH₂-CH₃). ¹⁹F NMR (CDCl₃) δ (ppm): 146.23. MS (MALDI-TOF): m/z = 1061.36 [M-F]⁺, 1061.45 calcd for C₆₄H₇₇BBr₂FN₂; MS (MALDI-TOF): m/z = 1080.35 [M]⁺, 1080.45 calcd for C₆₄H₇₇BBr₂F₂N₂. HR-MS (ESI): m/z = 1103.4437 [M+Na]⁺, 1103.4407 calcd for C₆₄H₇₇BBr₂F₂N₂Na. UV/Vis (CH₂Cl₂): λ_{max} (nm) (ε x 10⁻³ L mol⁻¹ cm⁻¹) = 242.0 (33.26), 253.0(34.04), 284.0 (63.69), 301.9.0 (70.91), 314.0 (129.19), 501.0 (104.18).

2,7-Di(4',4'-difluoro-1',3',5',7'-tetramethyl-4'-bora-3a',4a'-diazas-indacene)-

5,5',10,10',15,15'-hexabutyl-12-dibromotruxene (3). 2,4-Dimethylpyrrole (8 mmol, 0.76 g, 824.0 μL) and 5,5',10,10',15,15'-hexabutyl-7,12-dibromotruxene-2-dicarbaldehyde (2 mmol, 1.628 g) were dissolved in 100 mL of dry CH₂Cl₂ under a N₂ atmosphere. 50 μL of TFA was added at room temperature and the solution stirred overnight until TLC-control showed the complete consumption of the starting aldehyde. At this point, DDQ (4 mmol, 0.908 g) was added, stirring was continued for 60 min followed by the addition of 8 mL of Et₃N and 8 mL of BF₃·OEt₂ respectively. After stirring for 30 min the reaction mixture was washed with water, dried over Na₂SO₄ and evaporated to dryness. The residue was purified by column chromatography on silica gel with 60% DCM-heptane and 80% DCM-heptane. Yield: 103 mg, 4.1%. ¹H NMR (CDCl₃) δ (ppm): 8.53 (m, 2 H, truxene-*H*), 8.23 (d, 1 H, truxene-*H*), 7.63 (m, 1 H, truxene-*H*), 7.55 (m, 1 H, truxene-*H*), 7.48 (m, 2 H, truxene-*H*), 7.33 (m, 2 H, H-pyrro), 6.04(s, 4 H, H-pyrro), 3.02 (m, 6 H, H-truxene), 2.61 (s, 12 H, pyrro-CH₃), 2.12 (m, 6 H, Truxene-CH₂-), 1.51 (s, 12 H, pyrro-CH₃), 0.94 (m, 24 H, -CH₂-), 0.52 (m, 18 H, -CH₃). MS (MALDI-TOF): m/z = 1231.64 [M-F]⁺, 1231.09 calcd for C₇₇H₉₁B₂BrF₃N₄; m/z = 1248.64 [M]⁺, 1248.65 calcd for C₇₇H₉₁B₂BrF₄N₄. HR-MS (ESI): m/z = 1271.6461 [M+Na]⁺, 1271.6442 calcd for C₇₇H₉₁B₂BrF₄N₄Na. UV/Vis (CH₂Cl₂): λ_{max} (nm) (ε x 10⁻³ L mol⁻¹ cm⁻¹) = 251.9(66.11), 282.9 (88.16), 301.0 (102.14), 314.0 (164.47), 500.1 (245.88).

2,7-Di(4',4'-difluoro-1',3',5',7'-tetramethyl-4'-bora-3a',4a'-diazas-indacene)-12-(Zinc(II) 5,15-p-tolyl-10-phenylporphyrin)-5,5',10,10',15,15'-hexabutyltruxene (5). BODIPY **2** (0.0482 mmol, 52.2 mg, 1 equiv), borolanyporphyrin **4** (0.13 mmol, 95 mg, 2.6 equiv), potassium carbonate (150 mg, 1.085 mmol, 22 equiv) and tetrakis(triphenylphosphine)palladium(0) (5.56 mg, 0.00482 mmol, 0.1 equiv) were placed in a Schlenk tube and dissolved in toluene (10 mL) and H₂O (0.5 mL) under argon. The resulting solution was deoxygenated through three freeze-pump-thaw cycles and stirred at 96°C for 48 h. The solvent was removed and the residue was chromatographed on silica gel using CH₂Cl₂ as eluent. The crude product was further purified by column chromatography on silica gel with 60% CH₂Cl₂-heptane to afford the title compound in 33% yield (35 mg). ¹H NMR (CDCl₃) δ (ppm): 9.16 (d, 2 H, J = 6.0 Hz, H-pyrro), 9.13 (d, 2H, J = 6.0 Hz, H-pyrro), 9.10 (d, 2 H, J = 3.0 Hz, H-pyrro), 9.07 (d, 2 H, J = 3.0 Hz, H-pyrro), 9.03 (m, 4 H, H-pyrro), 8.82 (m, 4 H, truxene-H), 8.70 (m, 2 H, truxene-H), 8.49 (d, 1 H, J = 3.0 Hz, truxene-H), 8.45 (d, 1 H, J = 3.0 Hz, truxene-H), 8.30 (m, 6 H, H-phenyl), 8.20 (m, 8 H, H-phenyl and truxene), 7.79 (m, 6 H, H-phenyl and truxene), 7.60 (m, 9 H, H-phenyl and truxene), 7.40 (m, 1 H, H-truxene), 6.09 (s, 2 H, H-pyrro), 3.46 (m, 4 H, -CH₂-truxene), 3.25 (m, 2 H, -CH₂-truxene), 2.75 (s, 6 H, phenyl-CH₃), 2.74 (s, 6 H, phenyl-CH₃), 2.64 (s, 6 H, pyrro-CH₃), 2.53-2.27 (m, 6 H, truxene-CH₂-), 1.64 (s, 6 H, pyrro-CH₃), 1.29-1.07 (m, 24 H, -CH₂-), 0.93-0.69 (m, 30 H, -CH₃). ¹⁹F NMR (CDCl₃) δ (ppm): 146.16. MS (MALDI-TOF): m/z = 2176.91 [M]⁺, 2176.92 calcd for C₁₄₄H₁₃₁BF₂N₁₀Zn₂. HR-MS (ESI): m/z = 2199.9067 [M+Na]⁺, 2199.9094 calcd for C₁₄₄H₁₃₁BF₂N₁₀NaZn₂. UV/Vis (CH₂Cl₂): λ_{max} (nm) (ε x 10⁻³ L mol⁻¹ cm⁻¹) = 311.0 (60.06), 424.0 (687.52), 501.0 (67.62), 551.0 (33.60), 594.0 (12.18).

Instrumentation

¹H NMR spectra were recorded with a Bruker DRX-300 AVANCE transform spectrometer at the "Pôle Chimie Moléculaire (Welience, UB-Filiale)"; chemical shifts are expressed in ppm relative to chloroform. UV/Vis spectra were recorded with a Varian Cary 1 spectrophotometer. Mass spectra were obtained with a Bruker Daltonics Ultraflex II spectrometer in the MALDI/TOF reflectron mode using dithranol as a matrix or by ESI on a LTQ Orbitrap XL Thermo spectrometer. The measurements were made at the "Pôle Chimie Moléculaire (Welience, UB-Filiale)". UV-vis spectra were recorded on a Hewlett-Packard diode array model 8452A. Emission and excitation spectra were obtained using a double monochromator Fluorolog 2 instrument from Spex. Fluorescence and phosphorescence lifetimes were measured on a Timemaster Model TM-3/2003 apparatus from PTI,

incorporating a nitrogen laser as the source and a high-resolution dye laser (fwhm = 1.4 ns). Fluorescence lifetimes were obtained from high-quality decays and deconvolution or distribution lifetime analysis. The uncertainties ranged from 20 to 40 ps on the basis of multiple measurements. Phosphorescence lifetimes were determined using a PTI LS-100 incorporating a 1 μ s tungsten flash lamp (fwhm \sim 1 μ s). Flash photolysis spectra and transient lifetimes were measured using a Luzchem spectrometer using the 355 nm line of a YAG laser from Continuum (Serulite; fwhm =13 ns).

Quantum Yield Measurements

For measurements at 298 K, all samples were prepared in a glovebox, under argon ($O_2 < 12$ ppm), by dissolution of the compounds in 2MeTHF, using 1 cm³ quartz cells with a septum. Three different measurements (*i.e.*, different solutions) were performed for each set of photophysical data (quantum yield). The sample concentrations were chosen to correspond to an absorbance of \sim 0.05 at the excitation wavelength. Each absorbance value was measured three times for better accuracy in the measurements of emission quantum yields. Tetraphenylporphyrin zinc(II) (0.033 in THF) was used as reference.³⁴

DFT computations.

All density functional theory (DFT) and calculations were performed with Gaussian 09³⁵ at the Université de Sherbrooke with the Mammouth supercomputer supported by *Le Réseau Québécois De Calculs Hautes Performances*. The DFT geometry optimisations were carried out using the B3LYP method.³⁶⁻⁴⁵ A 6-31g* basis set was used for the BODIPY, porphyrin and truxene cycles while a 3-21g* basis set was used for all alkyl and aryl groups.⁴⁶⁻⁵¹ VDZ (valence double ζ) with SBKJC effective core potentials were used for all zinc atoms.⁴⁶⁻⁵¹

Femtosecond transient absorption spectroscopy.

The fs transient spectra and decay profiles were acquired on an homemade system using the SHG of a Soltice (Spectra Physics) Ti-Sapphire laser ($\lambda_{exc} = 398$ nm; FWHM = 75 ps; pulse energy = 0.1 μ J/pulse, rep. rate = 1 kHz; spot size \sim 500 μ m), a white light continuum generated inside a Sapphire window and a custom made dual CCD camera of 64 x 1024 pixels sensitive between 200 and 1100 nm (S7030, Spectronic Devices). The delay line permitted to probe up to 4 ns with an accuracy of \sim 4 fs. The results were analysed with the program Glotaran (<http://glotaran.org>) permitting to extract a sum of independent exponentials ($I(\lambda, t) = C_1(\lambda) \cdot \exp(-t/\tau_1) + C_2(\lambda) \cdot \exp(-t/\tau_2) + \dots$) that fits the whole 3D transient map.

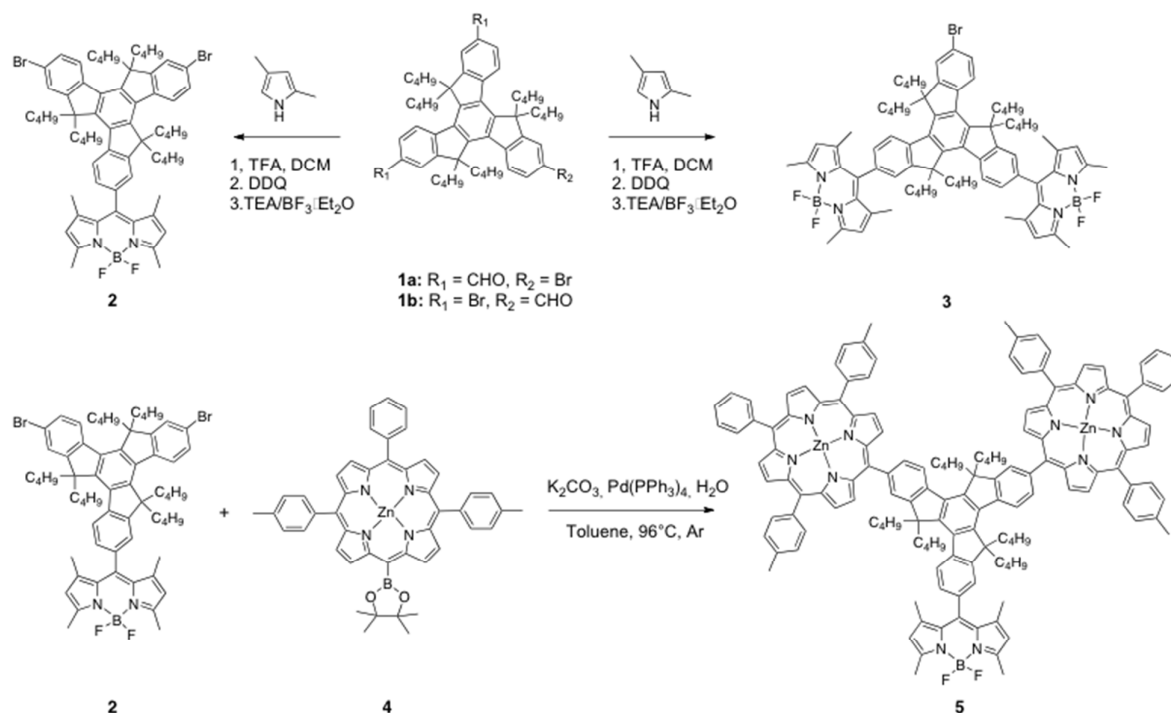
Fast kinetic fluorescence measurements

The short components of the fluorescence decays were measured using the output of an OPA (OPA-800CF, Spectra-Physics) operating at $\lambda_{\text{exc}} = 490$ nm, pulse width of 90 ps, rep. rate = 1 kHz, pulse energy = 1.6 $\mu\text{J}/\text{pulse}$, spot size ~ 2 mm, and a Streak Camera (Axis-TRS, Axis Photonique Inc.) with less than 8 ps resolution. The results were also globally analysed with the program Glotaran (<http://glotaran.org>) permitting to extract a sum of independent exponentials ($I(\lambda, t) = C_1(\lambda) \cdot \exp(-t/\tau_1) + C_2(\lambda) \cdot \exp(-t/\tau_2) + \dots$).

Results and discussion

Synthesis

Di- (**1a**) or monocarbaldehydehexabutyltruxene (**1b**) were prepared as previously described in the literature.^{18,19} The derivatives **2** and **3** were synthesized from the reaction of 5,5',10,10',15,15'-hexabutyl-7,12-dibromotruxene-2-carbaldehyde **1a** and 5,5',10,10',15,15'-hexabutyl-12-bromotruxene-2,7-dicarbaldehyde **1b** with 2,4-dimethylpyrrole in the presence of a catalytic amount of TFA (Scheme 1).



Scheme 1. Reaction paths to synthesize compounds **2**, **3** and **5**.

The condensation product obtained from the aldehyde and pyrrole was first oxidized with DDQ, followed by a neutralization with NEt₃, and subsequently was treated with BF₃·Et₂O to

afford the desired BODIPY compound **2** (17 %) and **3** (4%). The two resulting compounds display a strong greenish-yellow fluorescence in common organic solvents (chloroform, dichloroform, THF, and dioxane). The UV-visible spectra of the two BODIPY derivatives **2** and **3** show the presence of a characteristic sharp absorption maximum at 501 nm in dichloromethane due to the BODIPY moiety. Compound **5** was synthesized in 33% yield *via* the Suzuki coupling reaction of the BODIPY derivative **2** with borolanylporphyrin **4** in a toluene-water mixture in the presence of tetrakis(triphenylphosphine)palladium(0) as the catalyst and K₂CO₃ as the base (quenching the nascent acid generated during the reaction). Compound **5** is readily soluble in most solvents and displays also a characteristic BODIPY sharp absorption maximum at 501 nm in dichloromethane.

Spectroscopy and photophysics

The absorption, excitation and fluorescence spectra and spectroscopic and photophysical data for compounds **2**, **3**, and **5** are placed in Figure 1, Tables 1 and 2, respectively.

Table 1. UV-visible data for **2**, **3** and **5** in 2MeTHF.

Compd.	Peak maxima; absorption (nm)	Peak maxima; emission (nm)	Temp. (K)
2	285, 307, 374, 472, 500	507, 540	298
	283, 302, 309, 342, 365, 382, 470, 498	507, 542	77
3	280, 300, 312, 369, 387, 475, 499	513, 545	298
	286, 312, 370, 470, 490, 502	510, 550	77
5	407, 425, 487, 500, 560, 595	513, 608, 656	298
	412, 433, 470, 488, 502, 563, 606	510, 608, 667	77

Table 2. Photophysical data for **2**, **3**, **5**, and **6** in 2MeTHF.

Chrom. ^a	λ_{fluo} (nm)	τ_{F} (ns)	298K		77K		
			Φ_{F}	k_{ET} (s ⁻¹) (ET _{eff})	λ_{fluo} (nm)	τ_{F} (ns)	k_{ET} (s ⁻¹) (ET _{eff})
2 BODIPY	515, 540	5.03±0.10	0.59	□	515, 540	7.33±0.10	□
3 BODIPY	540	5.51±0.26	0.61	□	540	7.36±0.10	□
5 BODIPY	510	0.022±0.010	□	4.5 x 10 ¹⁰ (>99%)	510	0.038±0.10	2.6 x 10 ¹⁰ (98%)
[Zn]	665	1.66±0.10	□		670	1.92±0.10	
6 BODIPY	□	3.3		3.2 x 10 ⁷	□	4.6	9.4 x 10 ⁷
[Zn]	□	1.9	0.039	(11%)	□	2.3	(43%)

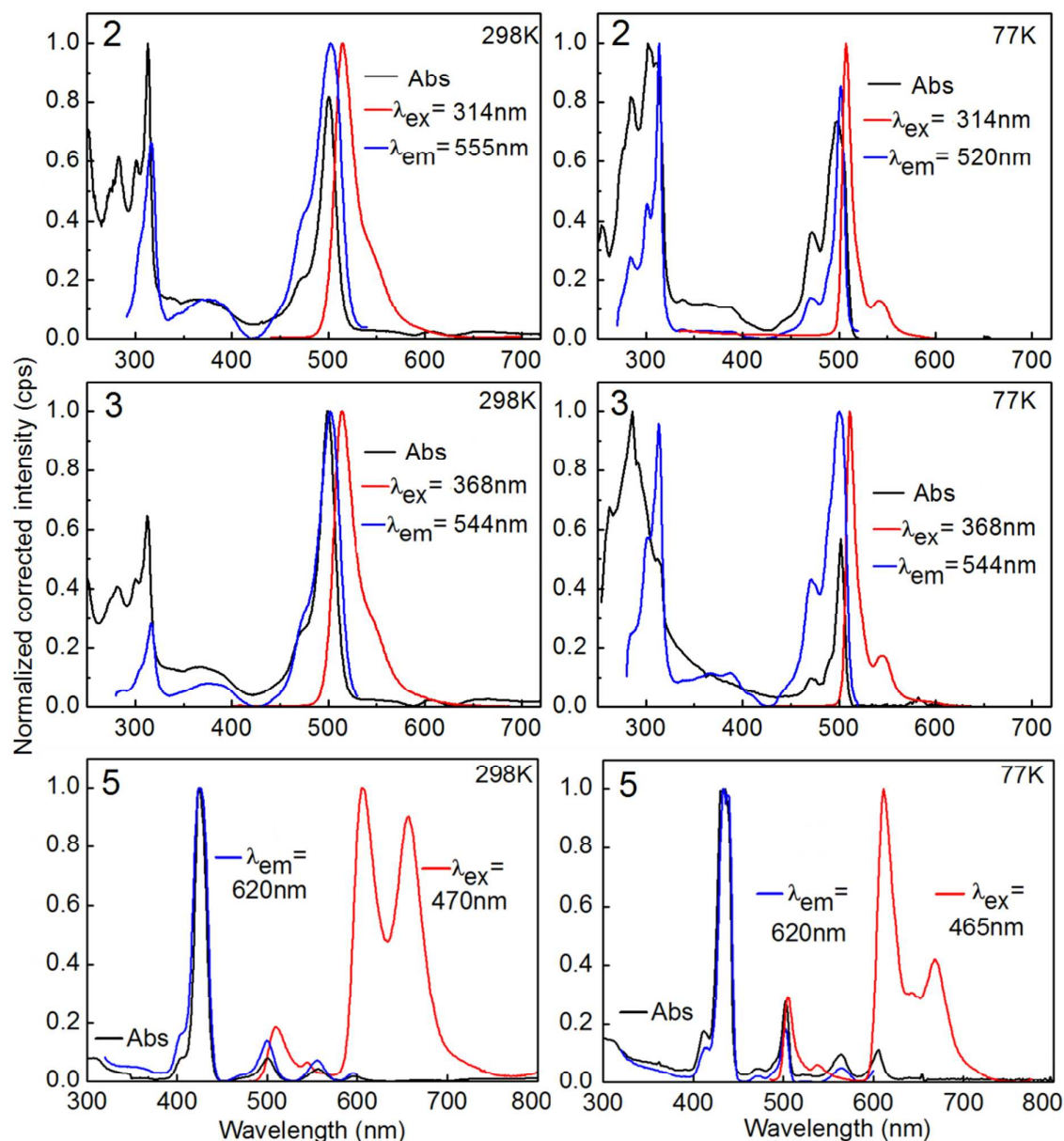


Figure 1. Absorption (black), excitation (blue) and fluorescence spectra (red) for **2**, **3** and **5** in 2MeTHF. The very weak signal at ~ 510 nm in compound **5** is that for the BODIPY fluorescence quenched by energy transfer to **[Zn]**. Note: the correction factor for the excitation spectra stops at 600 nm on this instrument.

The data for compounds **2** and **3** readily exhibit the characteristic features of the BODIPY chromophore^{1-12, 52-57} whereas those for compound **5** show the signatures of both the BODIPY and the zinc(II)porphyrin units, **[Zn]** (by comparison with the standard zinc(II)tetraphenylporphyrin (ZnTPP)).⁵⁸ In the context of this work, the assignment of the singlet energy donor (BODIPY) and acceptor (zinc(II)tetraarylporphyrin) is confirmed by the positions of the lowest energy peaks in the absorption and higher energy bands in the fluorescence spectra,

but also by the fast kinetic data provided below. The key feature of this analysis is the drastically weak fluorescence of the BODIPY chromophore in comparison to that for the zinc(II)tetraarylporphyrin one in compound **5** suggesting evidence for singlet energy transfer (*i.e.* $^1\text{BODIPY}^* \rightarrow [\text{Zn}]$). This hypothesis is readily supported by the good superposition of the excitation spectra with the absorption ones (Figure 1), which also indicates that this process is efficient. This observation is corroborated by the very small relative intensity (area under the curve) of the BODIPY fluorescence in **5** vs that of the acceptor (*i.e.* $\sim 1/8$; which indicates a relative fluorescence quantum yield of ~ 0.0049 at 298K; note that the fluorescence quantum yield for **3** is 0.61). This decrease is also reflected by the decrease in the fluorescence lifetime of the BODIPY chromophore (from 5.5 ns in **3** down to 22 ps in **5**, details are placed below).

Fast kinetics

The singlet energy transfer process was addressed by fs transient absorption (Figure 2) and fast time-resolved fluorescence spectroscopy using a Streak camera (Figure 3).

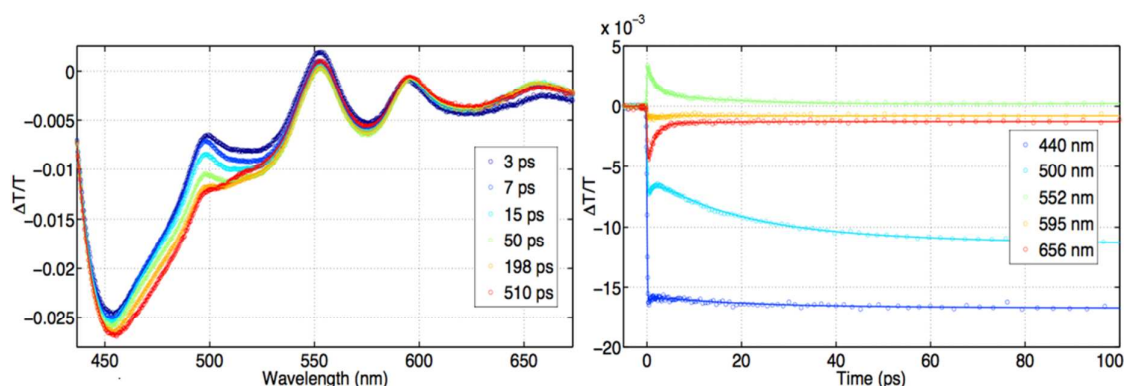


Figure 2. Left. Transient absorption spectra of **5** in 2MeTHF vs delay times. The signal at ~ 660 nm is stimulated fluorescence. Right. Decay profiles monitored at various wavelengths.

In Figure 2 (left), the traces are dominated by a photo-induced absorption signal (negative signal) that last for more than 4ns (maximum possible delay). This indicates that the final product is a triplet state of the **[Zn]** acceptor based on the striking resemblance with the spectrum of $^3\text{ZnTPP}^*$, which decays in the μs time scale with a maxima at ~ 460 nm.⁶⁴ The Q-bands at 550 and 590 nm are characteristic of the zinc(II)porphyrin.⁵⁹⁻⁶² The bleached signal at 500 nm is due to BODIPY.⁶³ The latter signal is the one that undergoes the largest intensity change upon delay times, indicating the presence of one or more fast processes. In all cases, a very fast component (~ 1.6 ps) is observed and unambiguously corresponds to a $S_2 \rightarrow S_1$ a process of the porphyrin ought to the selected excitation wavelength (398 nm) near the Soret band.⁶⁵ The other fast component is that of the BODIPY, which is readily depicted from the temporal profile of the 500 nm feature. Deconvolution of the decay traces provides a

reproducible value of 18.4 ps for this decay. Beside the 1.6 and 18.4 ps components, the other extracted values from the best fits are 1.86 ns (obviously associated with the porphyrin singlet excited lifetime), a longer component (> 4 ns; i.e. triplet state).

In order to confidently assign this kinetic behaviour of **5** in its excited states, fast fluorescence spectra were also examined. The reconstruction of the individual components from the graph fluorescence intensity vs wavelength vs time, were performed to show the contribution of the donor and the acceptor (Figure 3, left). The [Zn] emission was readily detected with negative coefficients at 610 nm, a behaviour commonly associated with energy transfer. At longer delay time, the fluorescence signal of the porphyrin unit (i.e. the acceptor) appears. The kinetic profile of the BODIPY monitored at 530 nm decays with a lifetime of 22 ps. Simultaneously, the zinc(II)porphyrin signal rises with a time constant of 22 ps as well. The correspondence between 18.4 (transient absorption decay) and 22 ps (fluorescence decay) is striking and is assigned to the BODIPY S_1 lifetime in **5**. At 77 K, this emission lifetime increase to 38 ps, in agreement with the increase in τ_{F° of **3** with the cooling of the temperature. During the course of this study, a weak component of 150 ps was also detected but could not be assigned with certainty.

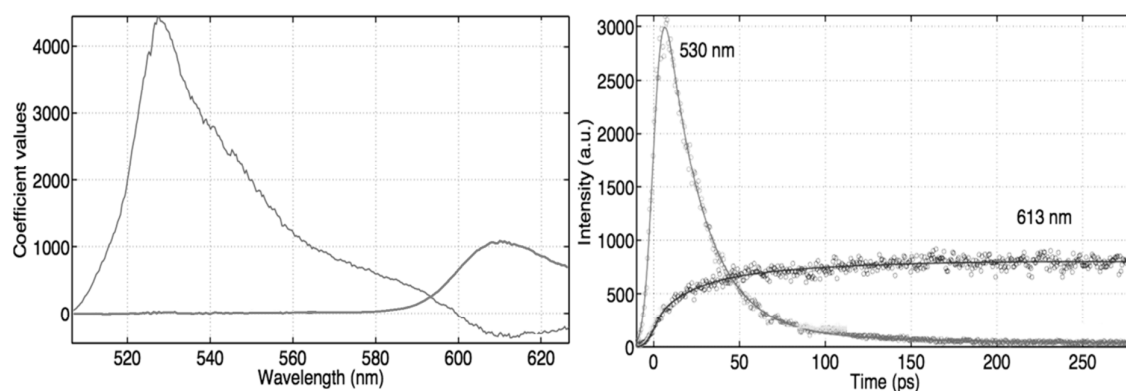


Figure 3. Left. Reconstruction of the fluorescence spectra from the decay traces of **5** in 2MeTHF at 298K (Figure 3).

Data analysis.

The efficiency, ET_{eff} , and rate for energy transfer, k_{ET} , can be extracted from the measurements of the fluorescence lifetime of the donor unit in the presence, τ_{F} , and absence of an acceptor, τ_{F° .⁵⁸ Both the Φ_{F° 's and τ_{F° 's for **2** and **3** are nearly constant indicating that the number of chromophores and Br-atoms (*via* a possible heavy atom effect) on the truxene base does not affect this parameter. This is consistent with the fact that the bromides are located far from the BODIPY chromophore. Moreover, the even shorter fluorescence

lifetimes reported by Ziessel and his collaborators,^{25,26} for the structurally related non-brominated BODIPY-C₆H₅C≡CH compound in acetonitrile ($\tau_F = 4.7$ ns) and CH₂Cl₂ ($\tau_F = 4.3$ ns) corroborate this conclusion. In compound **5**, τ_F decreases down to 22 and 38 ps, at 298 and 77 K, respectively, representing a decrease of 2 orders of magnitude in comparison with the τ_F 's. The k_{ET} (and ET_{eff}) parameters are more accurately calculated from $k_{ET} = (1/\tau_F) - (1/\tau_F^0)$ and $ET_{eff} = ((1/\tau_F) - (1/\tau_F^0))/(1/\tau_F)$.⁵⁸ These values are in the order of $4.5 \times 10^{10} \text{ s}^{-1}$ (99%) and $2.6 \times 10^{10} \text{ s}^{-1}$ (98%) at 298 and 77 K, respectively, and the k_{ET} values are consistent with other dyads recently reported in the literature (see compounds **7-10**, Figure 4),⁶⁶⁻⁷⁰ but about 2 orders of magnitude larger than those found for the structurally related dyad compound **6** (see Chart 1 and data in Table 2).¹³

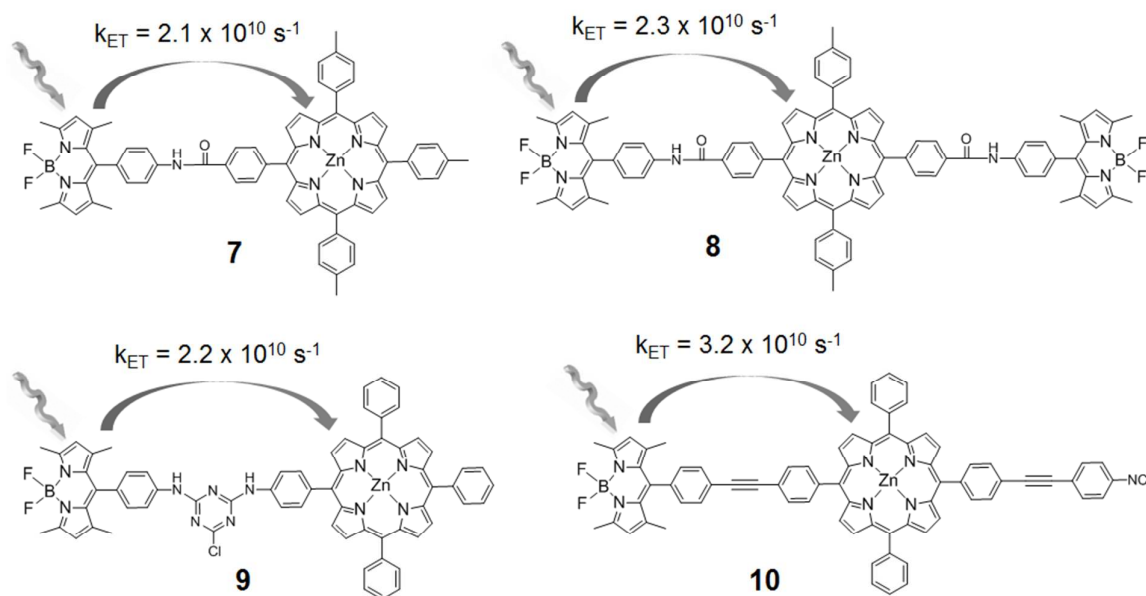


Figure 4. Structures and rates of singlet energy transfer dyads of some BODIPY-zinc(II)porphyrin dyads.

The fact that the k_{ET} and ET_{eff} parameters for **6** are significantly lower than those evaluated for compound **5** raises important questions. Computer modeling based on DFT computations (Figure 5) indicates that the center-to-center distances BODIPY-[Zn] are ~ 16 and ~ 12 Å, for **5** and **6**, respectively, intuitively meaning that k_{ET} for **6** at ~ 12 Å should have been faster. This last statement is based on the common approach that energy transfer rates are analysed using FRET, Förster Resonance Energy Transfer theory.¹⁴ This theory predicts that for long donor-acceptor interactions, k_{ET} is given by eq. 1:

$$(1) \quad k_{ET} = k_F^0(D) \cdot \frac{\kappa^2}{r^6} \cdot cte \cdot J$$

where $k_F^\circ(D)$ is the ratio $\Phi_F^\circ(D)/\tau_F^\circ(D)$ for the donor (D) in the absence of an acceptor (A), r is the center-to-center distance between the donor and the acceptor, κ^2 is an orientation factor between the transition moments of the donor and the acceptor ($\kappa^2 = (\sin\theta_D \cdot \sin\theta_A \cdot \cos\phi - 2 \cos\theta_D \cdot \cos\theta_A)^2$ with θ_D and θ_A being the angles formed between the transition moment vectors of D versus the center-to-center axis and of A and this same axis, and Φ being the dihedral angle made by the two transition moment vectors, and cte is the ratio $9000(\ln 10)/128\pi^5 n^4 N_a$ with n and N_a being the refractive index of the medium and Avogadro's number, respectively. In the case of porphyrin, the transition moments are doubly degenerated with two transition dipoles making an angle of 90° , κ^2 is then given by $\kappa^2 = (|\kappa(\nu)| + |\kappa(\nu + (\pi/2))|)^2/4$, where ν and $\nu + (\pi/2)$ represent ϕ for each component. Finally, the J integral is given by eq. 2:

$$(2) \quad J = \frac{\int F_D(\lambda) \epsilon_A(\lambda) \lambda^4 d\lambda}{\int F_D(\lambda) d\lambda}$$

where F_D is the fluorescence intensity of the donor and ϵ_A is the absorptivity of the acceptor.

The choice of the comparison molecule **6** is relevant for the purpose of this work since all structural parameters are kept reasonably similar. The $\Phi_F^\circ(D)$ and $\tau_F^\circ(D)$ parameters (Tables 1 and 2) remain about constants with respect to the BODIPY chromophore in **2** and **3**. Similarly, because the spectroscopic parameters (peak maxima and bandshapes) have not changed as well, the J-integral is also reasonably assumed to be approximately constant. Finally, the orientation factor components of eq. 1, κ^2 , should also be values within one order of magnitude since the lowest energy configurations of compounds **5** and **6** exhibit a helical geometry for both cases and that the dihedral angles made by the aromatic average planes are similar as well (i.e. difference of $15-20^\circ$; Figure 4). Indeed, the κ^2 values are within a factor of 2.5 at most (Table 3). In conclusion, the only parameter that plays a major role on the amplitude of k_{ET} is mostly r .

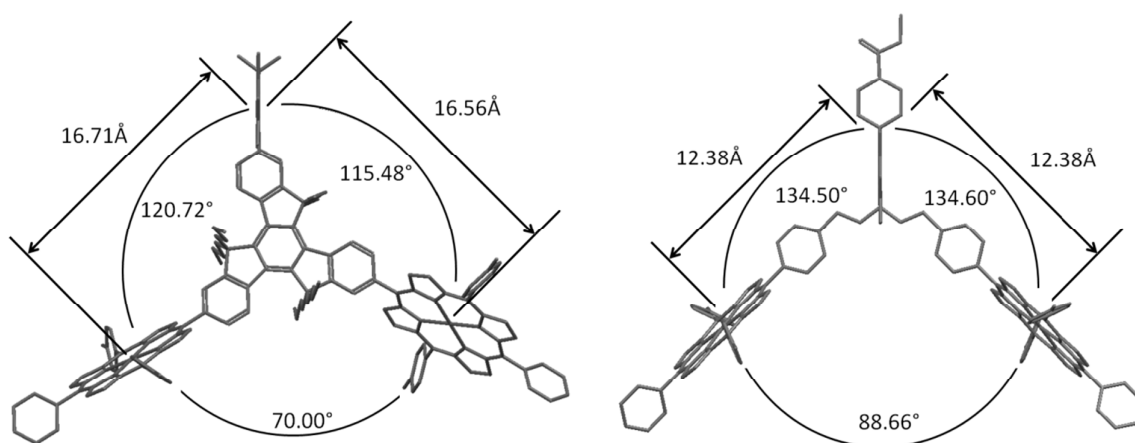


Figure 5. Optimized geometry (DFT; B3LYP) of **5** (left) and **6** (right). Only one enantiomer for each compound is shown for simplicity. The distances are the center-to-center separations, and the angles are those formed by the average planes between the BODIPY and porphyrin's.

Table 3. Structural parameters for the calculations of κ and κ^2 .

	θ_D	θ_A	ϕ_D	κ	κ^2
5 , BODIPY \rightarrow porphyrin 1, $\kappa(v)$	91.1	40.7	64.5	0.310	0.093
$\kappa(v+(\pi/2))$	91.1	130.7	64.5	0.301	
5 , BODIPY \rightarrow porphyrin 2, $\kappa(v)$	85.0	59.0	59.2	0.347	0.144
$\kappa(v+(\pi/2))$	85.0	149.0	59.2	0.412	
6 , BODIPY \rightarrow porphyrin 1, $\kappa(v)$	91.3	45.3	45.4	0.531	0.246
$\kappa(v+(\pi/2))$	91.3	135.3	45.4	0.462	
6 , BODIPY \rightarrow porphyrin 2, $\kappa(v)$	89.2	44.7	45.5	0.473	0.245
$\kappa(v+(\pi/2))$	89.2	134.7	45.5	0.518	

A simple examination of r^6 ($3.6 \times 10^6 \text{ \AA}^6$ for **6** vs $19.3 \times 10^6 \text{ \AA}^6$ for **5**) indicates that k_{ET} for **6** should have been at least 5 times faster than that for **5**. Similarly, the comparison of the κ^2 values suggests that k_{ET} for **6** should have been faster than that of **5** by a factor of 2.5. The even lower k_{ET} observed for **6** at 298 K ($3.2 \times 10^7 \text{ s}^{-1}$ making it ~ 2 orders of magnitude times slower than that for **7**), can tentatively be explained by the low thermal activation energy barrier allowing multiple conformations due to a facile rotation about the unconjugated $\text{CH}_2\text{-C}_6\text{H}_4$ bond. The result of this added flexibility is the access to a geometry where ϕ is $\sim 90^\circ$ where $\kappa^2 \sim 0$. The weighted average is then bound to lead to a slower k_{ET} . At 77K, the compounds try to reach the lowest energy configuration such as those presented in Figure 5. The temperature dependence on k_{ET} has also been examined before and one finds that linear relationships are more easily observed at 77 K versus 298 K.^{31,32,71} But the question still remains, why k_{ET} for **5** is drastically faster than that for **6**?

The only possible explanation is the presence of two processes in **5** and only one in **6**.

Compound **6** links the donor to the acceptor *via* a -B-O-CH₂-bridge which contains three unconjugated bonds. This structural feature clearly excludes the possibility of an energy transfer operating *via* a Dexter mechanism (*i.e.* double electron exchange which is bound to be strongly sensitive to orbital overlaps), by virtue of unreasonable distance for a through space process ($r > 5 \text{ \AA}$),^{31,32,72} and by the absence of π -conjugation in the bridge for a through bond process. Hence, this is leaving FRET as the only active mechanism in **6** (*i.e.* $k_{\text{ET}}(\mathbf{6}) = k_{\text{ET}}(\text{F\"orster})$, and $k_{\text{ET}}(\mathbf{5}) = k_{\text{ET}}(\text{F\"orster}) + k_{\text{ET}}(\text{Dexter})$). With this in hands, it appears possible to qualitatively evaluate the relative contribution of one mechanism *versus* the other in compound **5**. Since r is the major parameter that influences k_{ET} here, a simple calculation of k_{ET} in **6** as if it were $r = 16.56 \text{ \AA}$ (as in **5**) for example operating solely *via* a F\"orster process predicts that k_{ET} would be given by $(3.6 \times 10^6 / 20.6 \times 10^6) \times 9.4 \times 10^7 \text{ s}^{-1} \sim 1.6 \times 10^7 \text{ s}^{-1}$. This calculated anticipated contribution represents 1.3% of the observed value for **5** at 77 K ($2.6 \times 10^{10} \text{ s}^{-1}$). This observation indicates that the Dexter mechanism is clearly dominant in **5**.

In order to explain this phenomenon, DFT computations were performed to examine the frontier MOs of **5** and **6** (Figure 6) along with their fragment atomic contributions Table 4.

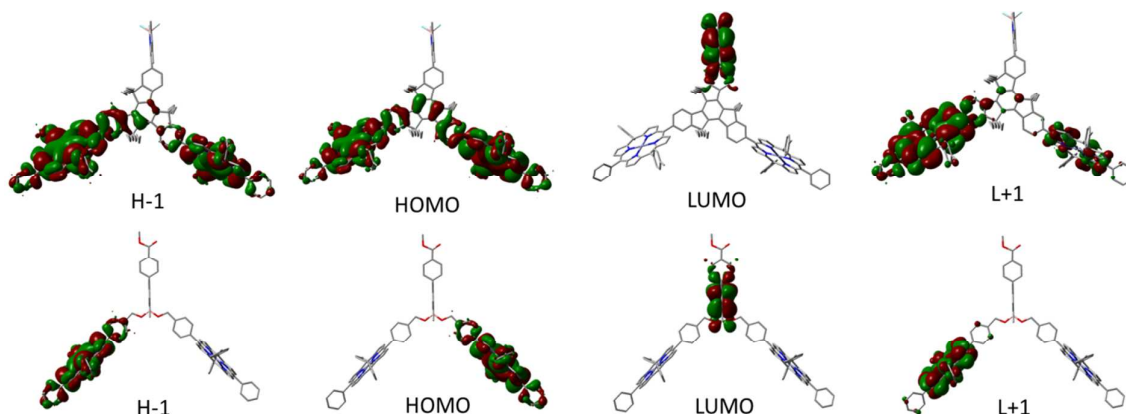


Figure 6. Representations of the frontier MOs for **5** and **6** (details are placed in the ESI).

Table 4. Contributions of the fragments to the frontier MOs of **5** (up) and **6** (down).

Fragment	HOMO-1	HOMO	LUMO	LUMO+1
BODIPY	0.01	0.00	82.67	0.00
Porphyrin 1	52.60	24.34	0.00	81.93
Porphyrin 2	25.29	52.42	0.00	4.70
Truxene	6.16	7.27	7.48	5.56
Aryls	15.93	15.97	9.85	7.80
Fragment	HOMO-1	HOMO	LUMO	LUMO+1
BODIPY + 2 C ₆ H ₄	3.8	3.9	80.5	1.1
Porphyrin 1	79.6	0.2	0.0	86.7
Porphyrin 2	0.2	79.6	0.0	0.0
Aryls	16.3	16.3	19.5	12.1

The key feature is that in both cases, the π -aryl and π -truxene groups participate to the atomic contributions of the frontier MOs (Figure 6) and their relative quantity are placed in Table 4. The alkyl group contributions are essentially nil. The calculated relative atomic contribution of the π -system of truxene of the HOMO and LUMO are >7% in **5** and secures some MO overlap between the L+1 (L = LUMO; centred on porphyrin 1 in this case) and LUMO (centred on BODIPY). Note that the filled MO of BODIPY is H-4 (H = HOMO; placed in the ESI). On the other hand, no atomic contribution is computed on the -O-CH₂- fragments for the frontier MO's of **6** (note that the contributions noted for the LUMO of **6** is that of the BODIPY π -system including the B-atom). The overall observation of these calculations is that the frontier MOs for **5** possesses the required orbital overlap for the double electron exchange (i.e. Dexter mechanism), and **6** does not, which corroborates the experimental findings.

One issue remains to be addressed. The k_{ET} values reported for **7-9** are those for seemingly unconjugated dyads. For **7-9**, the presence of NH functions permits electronic communication between the fragments as they would be conjugated, as recently well demonstrated for polyaniline models.⁷³

Conclusion

This work demonstrates that singlet energy transfer processes in a dyad built upon donor-truxene-acceptor operates mostly, not to say almost exclusively, *via* a Dexter mechanism (i.e. double electron transfer). The concept of a dual mechanism (Dexter *versus* Förster) is not new^{31,32} but its relative quantification is rare. Furthermore, this feature stresses the fact that k_{ET} is faster when the bridge is conjugated for dyads with the same donor-acceptor separation.

Acknowledgements

The “Centre National de la Recherche Scientifique” (ICMUB, UMR CNRS 6302) is gratefully thanked for financial support. Support was provided by the CNRS, the “Université de Bourgogne” and the “Conseil Régional de Bourgogne” through the 3MIM integrated project (“Marquage de Molécules par les Métaux pour l’Imagerie Médicale”). PDH thanks the Agence Nationale de la Recherche (ANR) and the Sciences and Engineering Research Council of Canada (NSERC) for financial support.

†Electronic Supplementary Information (ESI) available: HR-MS and ¹H NMR spectra of compounds **2**, **3** and **5**. See DOI: 10.1039/b000000x/

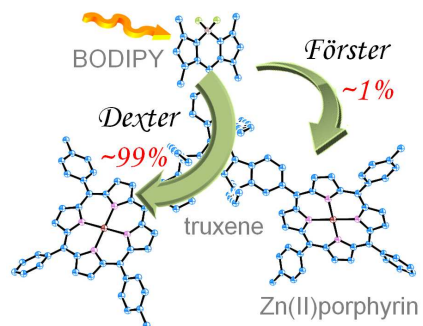
Notes and References

1. S. A. Baudron, *Dalton Trans.*, **2013**, 42, 7498-7509.
2. J. P. Lewtak and D. T. Gryko, *ChemComm*, **2012**, 48, 10069-10086.
3. G. Ulrich, R. Ziessel and A. Harriman, *Angew. Chem., Int. Ed.*, **2008**, 47, 1184-1201.
4. T. K. Khan, M. Broering, S. Mathur and M. Ravikanth, *Coord. Chem. Rev.*, **2013**, 257, 2348-2387.
5. V. Bandi, K. Ohkubo, S. Fukuzumi and F. D'Souza, *ChemComm*, **2013**, 49, 2867-2869.
6. F. D'Souza, A. N. Amin, M. E. El-Khouly, N. K. Subbaiyan, M. E. Zandler and S. Fukuzumi, *J. Am. Chem. Soc.*, **2012**, 134, 654-664.
7. A. Eggenspieler, A. Takai, M. E. El-Khouly, K. Ohkubo, C. P. Gros, C. Bernhard, C. Goze, F. Denat, J.-M. Barbe and S. Fukuzumi, *J. Phys. Chem. A*, **2012**, 116, 3889-3898.
8. T. K. Khan and M. Ravikanth, *Tetrahedron*, **2012**, 68, 830-840.
9. T. Lazarides, S. Kuhri, G. Charalambidis, M. K. Panda, D. M. Guldi and A. G. Coutsolelos, *Inorg. Chem.*, **2012**, 51, 4193-4204.
10. M. J. Leonardi, M. R. Topka and P. H. Dinolfo, *Inorg. Chem.*, **2012**, 51, 13114-13122.
11. W.-J. Shi, R. Menting, E. A. Ermilov, P.-C. Lo, B. Roeder and D. K. P. Ng, *ChemComm*, **2013**, 49, 5277-5279.
12. M. Shrestha, L. Si, C.-W. Chang, H. He, A. Sykes, C.-Y. Lin and E. W.-G. Diao, *J. Phys. Chem. C*, **2012**, 116, 10451-10460.
13. B. Brizet, A. Eggenspieler, C. P. Gros, J.-M. Barbe, C. Goze, F. Denat and P. D. Harvey, *J. Org. Chem.*, **2012**, 77, 3646-3650.
14. T. Förster, *Ann. Phys.*, **1948**, 2, 55-75.
15. D. L. Dexter, *J. Chem. Phys.*, **1953**, 21, 836-850.
16. H. K. Bisoyi and S. Kumar, *Chem. Soc. Rev.*, **2010**, 39, 264-285.
17. H. Zhang, D. Wu, S. H. Liu and J. Yin, *Curr. Org. Chem.*, **2012**, 16, 2124-2158.
18. B. Du, D. Fortin and P. D. Harvey, *Inorg. Chem.*, **2011**, 50, 11493-11505.
19. H.-J. Xu, B. Du, C. P. Gros, P. Richard, J.-M. Barbe and P. D. Harvey, *J. Porphyrins Phthalocyanines*, **2013**, 17, 44-55.
20. B. Du and P. D. Harvey, *ChemComm*, **2012**, 48, 2671-2673.
21. X.-F. Duan, J.-L. Wang and J. Pei, *Org. Lett.*, **2005**, 7, 4071-4074.
22. B. Du, D. Fortin and P. D. Harvey, *J. Inorg. Organomet. Pol. Mat.*, **2013**, 23, 81-88.
23. J.-M. Koenen, S. Jung, A. Patra, A. Helfer and U. Scherf, *Adv. Mat.*, **2012**, 24, 681-686.
24. J. Pina, J. S. Seixas de Melo, J.-M. Koenen, S. Jung and U. Scherf, *J. Phys. Chem. C*, **2013**, 117, 3718-3728.

25. S. Diring, F. Puntoriero, F. Nastasi, S. Campagna and R. Ziesse, *J. Am. Chem. Soc.*, **2009**, 131, 6108-6110.
26. S. Diring, B. Ventura, A. Barbieri and R. Ziesse, *Dalton Trans.*, **2012**, 41, 13090-13096.
27. S. Diring, R. Ziesse, F. Barigelletti, A. Barbieri and B. Ventura, *Chem. Eur. J.*, **2010**, 16, 9226-9236.
28. B. Ventura, A. Barbieri, F. Barigelletti, S. Diring and R. Ziesse, *Inorg. Chem.*, **2010**, 49, 8333-8346.
29. T. Bura, F. Nastasi, F. Puntoriero, S. Campagna and R. Ziesse, *Chem. Eur. J.*, **2013**, 19, 8900-8912.
30. M. D. Yilmaz, O. A. Bozdemir and E. U. Akkaya, *Org. Lett.*, **2006**, 8, 2871-2873.
31. S. Faure, C. Stern, R. Guilard and P. D. Harvey, *J. Am. Chem. Soc.*, **2004**, 126, 1253-1261.
32. W. G. Skene and S. Dufresne, *Org. Lett.*, **2004**, 6, 2949-2952.
33. B. Habermeyer, A. Takai, C. P. Gros, M. El Ojaimi, J.-M. Barbe and S. Fukuzumi, *Chem. Eur. J.*, **2011**, 17, 10670-10681.
34. D. R. Lide, *Handbook of Chemistry and Physics*, Chemical Rubber Publishing Co, Berlin, 1957.
35. M. J. Frisch *et al.* *Gaussian, Inc., Wallingford CT*, **2004**.
36. P. Hohenberg P and W. Kohn. *Phys. Rev.*, **1964**, 136, B864–871.
37. P. Hohenberg P and W. Kohn. *J. Phys. Rev.*, 1965; **140**: A1133–1138.
38. R. G. Parr and W. Yang, *Density-functional theory of atoms and molecules*, Oxford Univ. Press: Oxford, 1989.
39. D. R. Salahub and M. C. Zerner, *The Challenge of d and f Electrons*, Amer. Chem. Soc. Washington, D.C. 1989.
40. R. Bauernschmitt and R. Ahlrichs, *Chem. Phys. Lett.*, **1996**, 256, 454–464.
41. M. E. Casida, C. Jamorski, K. C. Casida and D. R. Salahub, *J. Chem. Phys.*, **1998**, 108, 4439–4449.
42. R. E. Stratmann, G. E. Scuseria and M. J. Frisch, *J. Chem. Phys.*, **1998**, 109, 8218–8224.
43. C. Lee C, Yang W and Parr RG. *Phys. Rev. B*, **1988**, 37, 785–789.
44. B. Miehlich, A. Savin, H. Stoll and H. Preuss, *Chem. Phys. Lett.*, **1989**, 157, 200–206.
45. A. D. Becke, *J. Chem. Phys.*, **1993**, 98, 5648–5652.
46. J. S. Binkley, J. A. Pople and W. J. Hehre, *J. Am. Chem. Soc.* **1980**, 102, 939–947.

47. M. S. Gordon, J. S. Binkley, J. A. Pople, W. J. Pietro and W. J. Hehre, *J. Am. Chem. Soc.* **1982**, 104, 2797–2803.
48. W. J. Pietro, M. M. Francl, W. J. Hehre, D. J. Defrees, J. A. Pople and J. S. Binkley, *J. Am. Chem. Soc.* **1982**, 104, 5039–5048.
49. K. D. Dobbs and W. J. Hehre, *J. Comput. Chem.* **1986**, 7, 359–378.
50. K. D. Dobbs and W. J. Hehre, *J. Comput. Chem.* **1987**, 8, 861–879.
51. K. D. Dobbs and W. J. Hehre, *J. Comput. Chem.* **1987**, 8, 880–893.
52. Y. Chen, L. Wan, X. Yu, W. Li, Y. Bian and J. Jiang, *Org. Lett.*, **2011**, 13, 5774–5777.
53. T. K. Khan and M. Ravikanth, *Eur. J. Org. Chem.*, **2011**, 34, 7011–7022.
54. T. K. Khan and M. Ravikanth, *Tetrahedron*, **2011**, 67, 5816–5824.
55. T. Lazarides, G. Charalambidis, A. Vuillamy, M. Reglier, E. Klontzas, G. Froudakis, S. Kuhri, D. M. Guldi and A. G. Coutsolelos, *Inorg. Chem.*, **2011**, 50, 8926–8936.
56. J. Warnan, F. Buchet, Y. Pellegrin, E. Blart and F. Odobel, *Org. Lett.*, **2011**, 13, 3944–3947.
57. M. T. Whited, P. I. Djurovich, S. T. Roberts, A. C. Durrell, C. W. Schlenker, S. E. Bradforth and M. E. Thompson, *J. Am. Chem. Soc.*, **2011**, 133, 88–96.
58. P. D. Harvey, in *The Porphyrin Handbook*, eds. K. M. Kadish, K. M. Smith and R. Guilard, Boston, 2003, p. 63.
56. M. Andersson, J. Davidsson, L. Hammarstroem, J. Korppi-Tommola, and T. J. Peltola, *Phys. Chem. B*, **1999**, 103, 3258–3262.
60. M. Enescu, K. Steenkeste, F. Tfibel, and M-P. Fontaine-Aupart, *Phys. Chem. Chem. Phys.*, **2002**, 4(24), 6092–6099.
61. R. T. Hayes, C. J. Walsh, and M. R. Wasielewski, *J. Phys. Chem. A.*, **2004**, 108(13), 2375–2381.
62. A. Gabrielsson, F. Hartl, H. Zhang, J. R. Lindsay Smith, M. Towrie, A. Vlcek Jr., and R. N. Perutz, *J. Am. Chem. Soc.* **2006**, 128(13), 4253–4266.
63. D. W. Cho, M. Fujitsuka, J. H. Ryu, M. H. Lee, H. K. Kim, T. Majima, and C. Im, *Chem. Commun.*, **2012**, 48(28), 3424–3426.
64. S. Funakura, K. Nakatani, H. Misawa, N. Kitamura, and H. Masuhara, *J. Phys. Chem.* **1995**, 99(41), 15192–15197.
65. a) U. Tripathy, D. Kowalska, X. Liu, S. Velate, and R. P. Steer, *J. Phys. Chem. A* **2008**, 112, 5824–5833. b) H-Z. Yu, S. J. Baskin, A. H. Zewail, *J. Phys. Chem. A.*, **2002**, 106(42), 9845–9854.

66. T. Lazarides, S. Kuhri, G. Charalambidis, M. K. Panda, D. M. Guldi, and A. G. Coutsolelos, *Inorg. Chem.*, **2012**, 51(7), 4193-4204.
67. T. Lazarides, G. Charalambidis, A. Vuillamy, M. Reglier, E. Klontzas, G. Froudakis, S. Kuhri, D. M. Guldi, and A. G. Coutsolelos, *Inorg. Chem.*, **2011**, 50(18), 8926-8936.
68. M. T. Whited, P. I. Djurovich, S. T. Roberts, A. C. Durrell, C. W. Schlenker, S. E. Bradforth, and M. E. Thompson, *J. Am. Chem. Soc.*, **2011**, 133(1), 88-96.
69. E. Maligaspe, T. Kumpulainen, N. K. Subbaiyan, M. E. Zandler, H. Lemmetyinen, N. V. Tkachenko, and F. D'Souza, *Phys. Chem. Chem. Phys.*, **2010**, 12(27), 7434-7444.
70. C. Y. Lee, J. K. Jang, C.H. Kim, J. Jung, B.K. Park, J. Park, W. Choi, Y-K Han, T. Joo, J. T. Park, *Chem. Euro. J.*, **2010**, 16(19), 5586-5599.
71. J.-M. Camus, S. M. Aly, C. Stern, R. Guillard and P. D. Harvey, *ChemComm*, **2011**, 47, 8817-8819.
72. S. Faure, C. Stern, E. Espinosa, R. Guillard and P. D. Harvey, *Chem. Eur. J.*, **2005**, 11, 3469-3481.
73. X. Wang, D. Fortin, G. Brisard, P. D. Harvey, *ChemComm*, **2014**, 50, 350-352.



BODIPY uses the truxene bridge to transfer its S_1 energy to the zinc(II)porphyrin acceptors via a Dexter mechanism almost exclusively.